Noname manuscript No.
(will be inserted by the editor)

Minimalistic Control of Biped Walking in Rough Terrain

Fumiya Iida · Russ Tedrake

Received: date / Accepted: date

Abstract The compass gait model has been intensively studied for a systematic investigation of complex biped locomotion dynamics, while most of the previous studies focused only on the locomotion on flat surfaces. In order to take a significant step forward in the study of dynamic biped walking, the problem addressed in this paper is the minimalistic control architecture of the compass gait model for walking in rough terrains. This controller utilizes an open-loop sinusoidal oscillation of hip motor, which induces basic walking stability without sensory feedback. A set of simulation analyses show that the underlying mechanism of the minimalistic controller lies in the "phase locking" mechanism that compensates phase delays between mechanical dynamics and the open-loop motor oscillation resulting in a relatively large basin of attraction in dynamic bipedal walking. By exploiting this mechanism, we also explain how the basin of attraction can be controlled by manipulating the parameters of oscillator not only on a flat terrain but also in various inclined slopes. Based on the simulation analysis, the proposed controller is implemented in a real-world robotic platform to confirm the plausibility of the approach. In addition, by using these basic principles of self-stability and gait variability, we demonstrate how the proposed controller can be extended with a simple sensory feedback such that the robot is able to control gait patterns autonomously for traversing a rough terrain.

Keywords Dynamic legged locomotion · Biped robot · Passive dynamics · Compass gait model

F. Iida · R. Tedrake
Computer Science and Artificial Intelligence Laboratory, Massachusetts Institute of Technology, 32 Vassar Street, Cambridge, MA, 02139 USA. E-mail: iida@csail.mit.edu, russt@mit.edu

1 Introduction

Since the pioneering work of the Passive Dynamic Walkers (PDWs: [1,2]), the problem of dynamic walking has attracted a number of researchers in order to understand and improve locomotion capabilities of legged robots. If compared with fully actuated legged robots, the use of passive dynamics is expected not only to substantially increase energy efficiency but also to obtain additional insights into natural walking dynamics. Previously it has been demonstrated that the use of passive dynamics leads to energetically efficient dynamic locomotion [3–6] as well as mechanically self-stabilizing locomotion dynamics [8,7]. Despite these high impact demonstrations in the past, control of the PDWs appears to be a challenging problem because of the nonlinearity originated in complex mechanical dynamics, and the locomotion capabilities of these robots are still restricted in a flat environment.

In order to obtain an in-depth understanding of dynamic bipedal walking, the so-called compass gait walking model (also known as the simplest walking model) has been intensively studied [9]. An important aspect of this model lies in the fact that it is irreducibly simple and analytically tractable, which enable us systematically investigate both mechanical interactions and dynamic behavior control. Previously, the compass gait model was investigated in terms of mechanical interactions in a passive regime [1,10,11], and its variations were developed for investigating, for example, knee dynamics and locomotion stability [12–16], shapes and actuation of foot segments [17–21], mass distribution [22], and lateral balancing [23]. Control architectures for the compass gait model have also been studied with respect to energy based optimal control [24–30], phase resetting mechanisms [31–33], and control optimization in

rough terrains [34,35]. Through these previous studies on the compass gait model and its variations, we have gained accumulated knowledge about the stability and controllability, whereas most of the studies above were conducted in flat environment or only in simulation.

From this perspective, the primary goal of this paper is to take a significant step forward to real-world experimentation of the compass gait model in rough terrains by investigating the minimalistic control architecture. The controller makes use of an open-loop sinusoidal oscillation of motor torque exerted at the hip joint, and through a set of simulation analyses and real-world experiments, we explain how this controller deals with undesired deviations of trajectories while keeping the controllability of locomotion dynamics, which are two essential components for legged locomotion in rough terrains. More specifically, we found that the open-loop controller is not only beneficial for the real-world implementation because of no necessity of state feedback, but also capable of inducing a "phase locking" mechanism, that is, undesired phase delays between walking dynamics and motor oscillation can be compensated without any explicit control. As a result, owing to the phase locking mechanism, walking dynamics can be harnessed around a relatively large basin of attraction. Furthermore, we also explain how the walking dynamics can be manipulated by the parameters of motor oscillation, resulting in control of stride length not only in a flat surface but also in various inclined slopes.

For a real-world evaluation of the proposed control approach, we developed a robotic platform based on the original compass gait model. Although dynamics of the robotic platform is slightly different from the simulation model due to the physical constraints in the real world, we show that the novel characteristics of the proposed controller (i.e. self-stability and gait variability) are preserved. And finally, we extend the minimalistic control architecture with a minimum sensory feedback, and we demonstrate that the proposed controller can take advantage of the intrinsic stability and gait variability to autonomously navigate through a relatively complex rough terrain.

2 Control of a Compass Gait Model

For a systematic investigation of the minimalistic control architecture, this section first introduces the compass gait model and basic assumptions of the controller. Then the underlying mechanism of self-stability is explained through a set of simulation experiments.

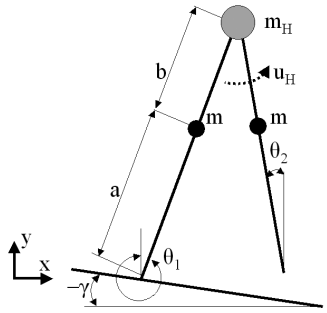

Fig. 1 Compass Gait Model. A point mass m_H is defined at the hip joint, which is actuated by motor torque u_H. Black circles denote the centers of leg mass, which are determined by a and b.

Table 1 Specification of Simulation Model

Symbol	Description	Value
a	Lower Leg Segment	0.5 m
b	Upper Leg Segment	0.5 m
m	Mass of Leg	5.0 kg
m_H	Mass of Body	5.0 kg
g	Gravitational Constant	$9.8m/s^2$

2.1 Compass Gait Model

The compass gait model consists of two sets of dynamics: a continuous dynamics of swing leg and a transition dynamics that occurs at the event of touchdown and switching of the swing and stance legs.

The swing-leg dynamics of the compass gait model can be described as follows.

$$M(q)\ddot{q} + C(q,\dot{q})\dot{q} + G(q) = Bu \tag{1}$$

$$M(q) = \begin{bmatrix} mb^2 & -mblcos(\theta_1-\theta_2) \\ -mblcos(\theta_1-\theta_2) & ma^2+m_Hl^2+ml^2 \end{bmatrix}$$
$$C(q,\dot{q}) = \begin{bmatrix} 0 & mblsin(\theta_1-\theta_2)\dot{\theta}_1 \\ -mblsin(\theta_1-\theta_2)\dot{\theta}_2 & 0 \end{bmatrix}$$
$$G(q) = \begin{bmatrix} mgbsin\theta_2 \\ -mgasin\theta_1 - m_Hglsin\theta_1 - mglsin\theta_1 \end{bmatrix}$$
$$B = \begin{bmatrix} 1 & 1 \\ 0 & -1 \end{bmatrix}$$

where $q = [\theta_1, \theta_2]^T$, $u = [u_H, 0]^T$ (u_H is torque generated by the hip actuator), and $l = a + b$ (see Table 1 for specifications).

When the state variables satisfy $\theta_1 - \theta_2 = \gamma$, the swing-leg dynamics is terminated, and the collision dynamics is computed as follows. At the ground contact of the swing leg and switching to the stance leg, the compass gait model assumes the conservation of angu-

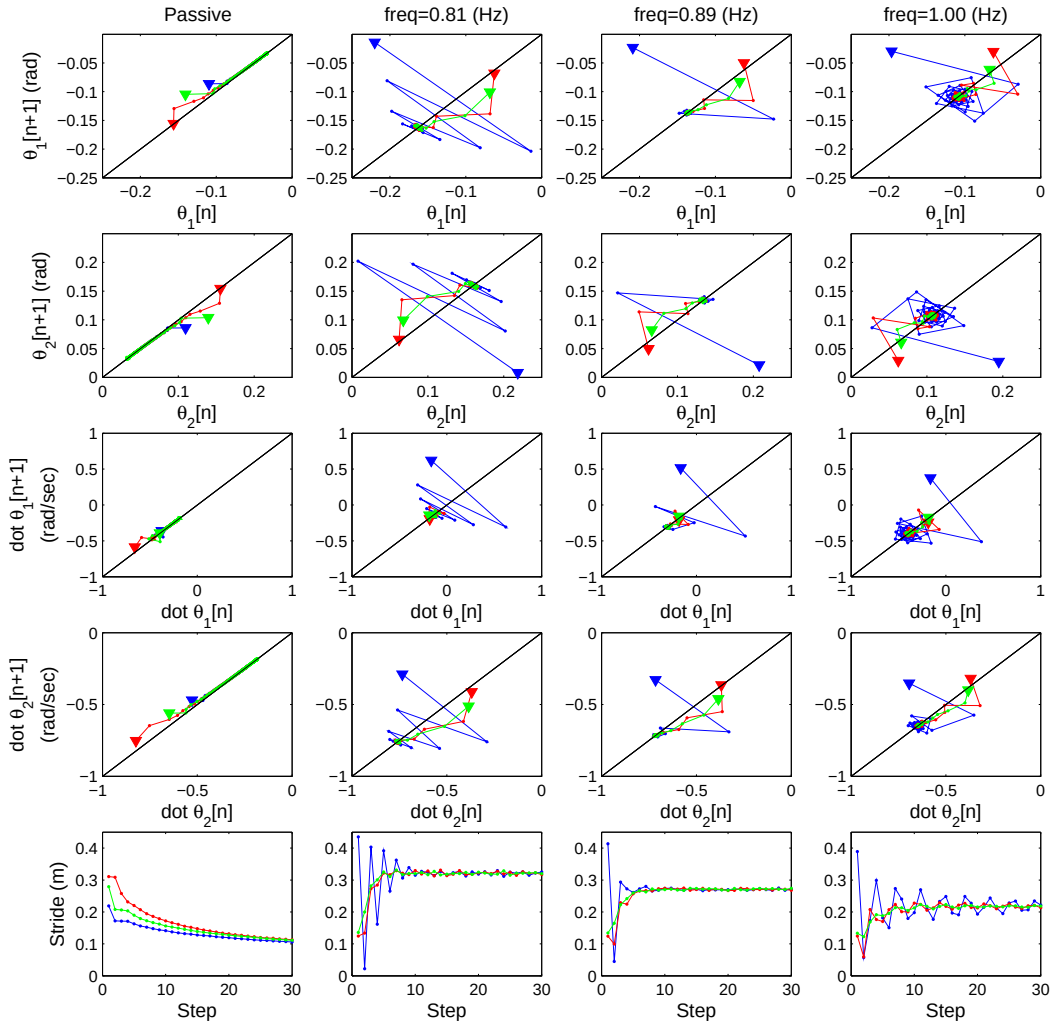

Fig. 2 Projections of the return map of the compass gait simulation with and without hip actuation. These projections depict the state variables ($q = [\theta_1, \theta_2]^T$ and $q = [\dot{\theta}_1, \dot{\theta}_2]^T$ at every touchdown of the swing leg, and three trajectories starting from different initial conditions (indicated by colored triangle plots) are shown in every diagram. Stride length of every walking step is plotted in the lower figures, where stride length is decreased gradually without hip actuation while it converges to a certain value with the hip actuation.

lar momentum around the hip joint and the toe of the swing leg.

$$Q_p \dot{q}^+ = Q_m \dot{q}^- \tag{2}$$

$$Q_p = \begin{bmatrix} mb^2 - mblcos2\alpha & ml^2 + m_H l^2 + ma^2 - mblcos2\alpha \\ mb^2 & -mblcos2\alpha \end{bmatrix}$$

$$Q_m = \begin{bmatrix} -mab & -mab + (m_H l^2 + 2mal)cos2\alpha \\ 0 & -mab \end{bmatrix}$$

$$\alpha = \frac{\theta_1^- - \theta_2^-}{2}$$

where Q_p and Q_m represent transition matrices between swing and stance legs, + and − signs denote the state variables right after and right before the swing leg touchdown.

In this paper, we consider a minimalistic control strategy in which an open-loop motor controller plays an important role to induce self-stabilizing walking dynamics. The controller uses a sinusoidal oscillator with no sensory feedback. More specifically, torque of the hip motor u_H is determined as follows:

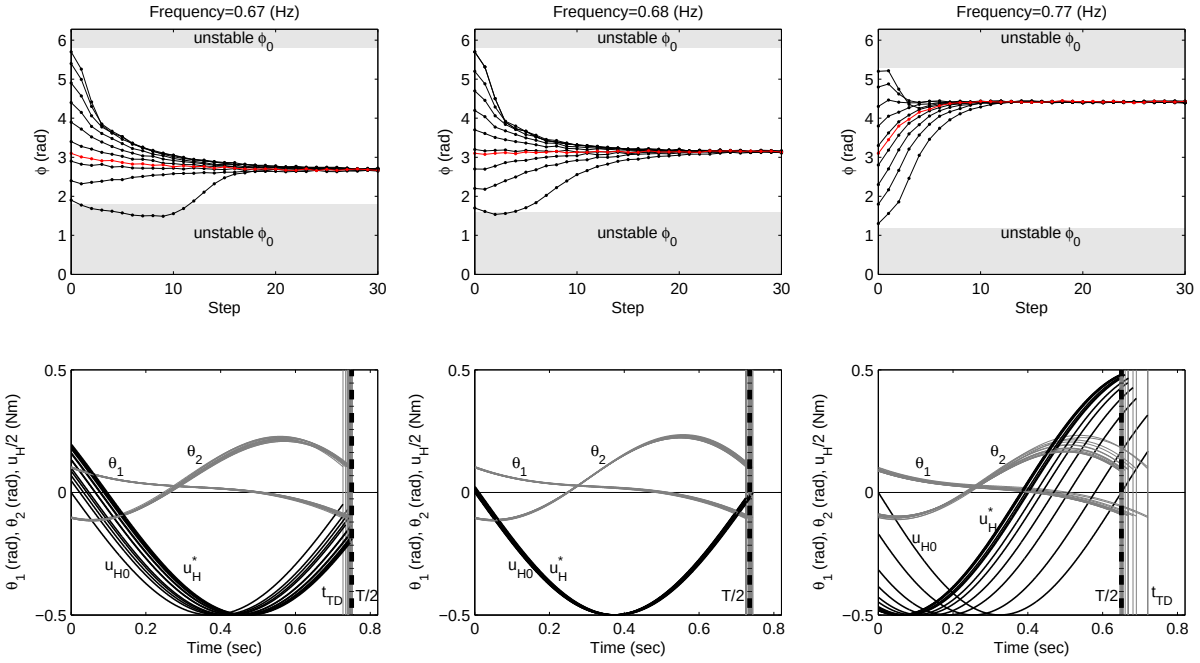

Fig. 3 The compass gait simulation with different frequency parameters. Upper figures show basins of attraction with respect to different initial phase delays ϕ_0 in hip actuation. The detailed walking dynamics starting from $\phi_0 = \pi$ (highlighted by the red lines) are shown in lower figures. These figures illustrate time series trajectories of state variables q (gray curves), hip motor torque u_H (black curves), and the time of collision t_{TD}. In left and right figures, t_{TD} converges to the period of hip motor oscillation $\frac{T}{2}$ (represented by the broken lines), which indicates the phase locking. In these simulation, the amplitude parameter is fixed at $A = 1.0$ (Nm).

$$u_{Hn}(t) = A_n sin(2\pi f_n t + \phi_{n-1}) \tag{3}$$

where A_n and f_n are amplitude and frequency parameters at step n that determine hip joint torque. Note that, in the rest of this paper, we consider an open-loop controller which varies the control parameters only at the end of every oscillation cycle. The variable ϕ_{n-1}, therefore, represents the phase delays of the oscillator cycle at the moment of touchdown of the swing leg.

2.2 Basin of Attraction

Basic locomotion stability of the compass gait model is shown in Fig. 2, which depicts projections of the return map. These figures illustrate all state variables of the model at the moments of touchdown while walking on a flat terrain with different oscillation of the hip motor explained above. The most extreme case of stability is shown in the left most plots, in which the model exhibits steady periodic walking even with the hip motor torque set to zero. More specifically, although stride length is decreased for the energy loss at every touchdown, all trajectories starting from three different initial conditions follow the fix points of state variables all the way until it falls over with the stride close to zero.

In contrast, the compass gait model exhibits a steady periodic locomotion with the energy input through the sinusoidal oscillation of hip motor. For example, Fig. 2 also shows three different frequency values of the hip oscillation, and the locomotion processes starting from different initial conditions converge to the same fix point and a constant stride length that is uniquely defined by the frequency parameter.

For more detailed analysis of the locomotion process, we investigate one step dynamics, which can be described as follows:

$$\begin{bmatrix} q_{n+1}^+ \\ \dot{q}_{n+1}^+ \\ \phi_{n+1} \end{bmatrix} = S(q_n^+, \dot{q}_n^+, \phi_n, f_n, A_n) \tag{4}$$

$$\phi_{n+1} = \phi_n - (\frac{T_n}{2} - t_{TD}) \cdot 2\pi f_n \tag{5}$$

$$T_n = \frac{1}{f_n} \tag{6}$$

where the function S computes the swing leg dynamics (Eq. (1)) and the collision dynamics (Eq. (2)), given q_n^+

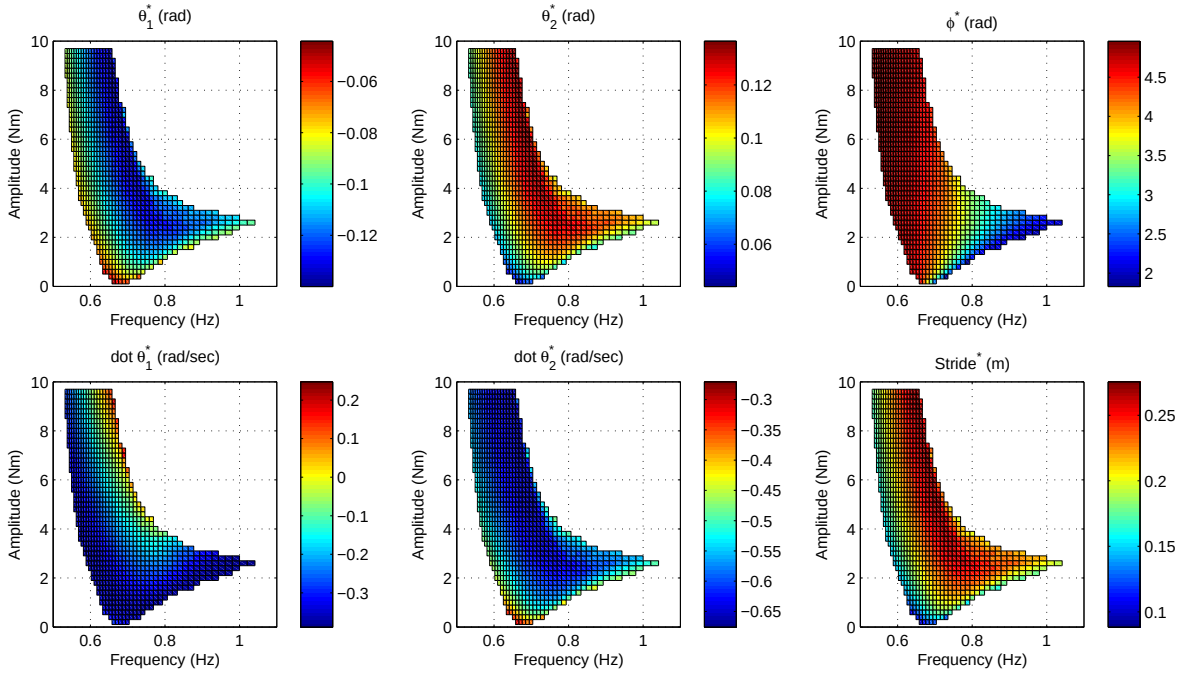

Fig. 4 State variables, phase delays, and stride lengths at fix points on a flat terrain with respect to the control parameters A and f. $Stride^*$ is calculated based on $q^* = [\theta_1^*, \theta_2^*]^T$ and the leg length l.

and $\dot{q}_n^+$ representing the state variables right after the collision of the swing leg in step $n-1$. t_{TD} indicates the duration between previous and current collisions, and A_n, f_n and T_n are the amplitude, frequency, and period of hip motor oscillation, respectively (see Eq. (3)). A fix point can, therefore, be described as follows:

$$\begin{bmatrix} q^* \\ \dot{q}^* \\ \phi^* \end{bmatrix} = S(q^*, \dot{q}^*, \phi^*, f, A) \tag{7}$$

Fig. 3 (upper figures) shows how variations of initial phase delays ϕ_0 converge to the phase delay at the fix point ϕ^*, which essentially indicates the basin of attraction around the fix point. For example, with the frequency parameter 0.67 Hz, the locomotion process starting from an initial phase delay $\phi_0 = 5.5$ (rad) converges to $\phi^* = 2.9$ (rad) after approximately 15 steps. As shown in these figures, the basins of attraction are generally large enough that a significant deviation of phase delay can converge to the fix point. More detailed trajectories of walking dynamics can be analyzed through the state variables and motor torque, which is also shown in Fig. 3 (lower figures). These figures illustrate the simulation started from an initial phase delay $\phi_0 = \pi$ for all three frequency parameters. Here we clearly observe "phase locking" mechanism, that is, a time of collision t_{TD} converges to the period of motor oscillation $\frac{T}{2}$, and accordingly the phase delay ϕ (computed by Eq. (5)) converges to ϕ^*.

It is important to note that, through these simulation experiments, we always found only one unique fix point $[q^*, \dot{q}^*, \phi^*]^T$ when the control parameters f and A are specified. Also another interesting characteristic shown in Fig. 3 (upper figures) is that it requires more steps to converge when an initial phase delay is smaller than the fix point, if compared with starting from larger ones. In addition, as a natural consequence of the phase locking mechanism, similar basins of attraction can also be observed when started from some deviations of the other initial parameters, i.e. q_0^+ and $\dot{q}_0^+$.

2.3 Control of Fix Point

So far we discussed how the frequency parameter of hip motor oscillation is related to fix points of walking dynamics, but fix points can also be influenced by the other parameters of the compass gait model. This section explores an entire landscape of model parameters including the amplitude of oscillator A and the slope angle γ, which is necessary to obtain a basic characteristics of the proposed control framework.

The first set of simulation was conducted on a flat ground $\gamma = 0$ (rad), and we searched fix points with re-

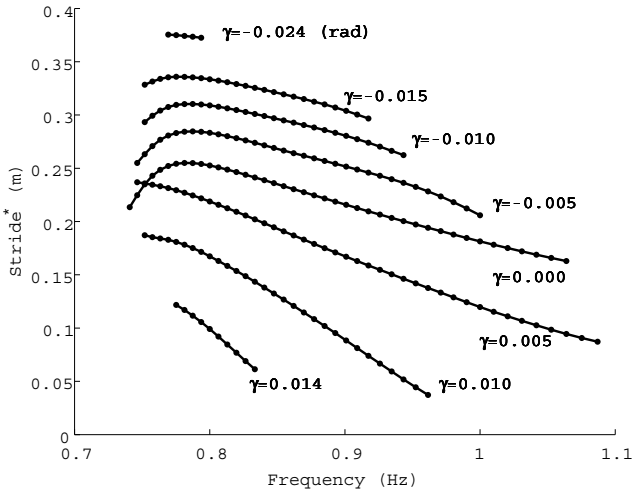

Fig. 5 Stride length at the fix points determined by frequency parameter f and slope angles γ ($\gamma < 0$ indicates downhill slopes). Amplitude parameter is fixed at $A = 7.0$ (Nm).

spect to both control parameters A and f. As explained in the previous subsection, each fix point (represented by q^*, $\dot{q}^*$, ϕ^*) can be uniquely found once we set these control parameters, and the result is shown in Fig. 4. Note that, once a fix point is found, we are also able to estimate stride length of the fix point $Stride^*$, which is an important metric to determine footholds during locomotion in rough terrain. From the state variable $q^* = [\theta_1^*, \theta_2^*]^T$, $Stride^*$ can be estimated as follows:

$$Stride^* = l(cos\theta_1^* + cos\theta_2^*) \tag{8}$$

In general, from the figure of $Stride^*$ (lower right figure in Fig. 4), it is shown that stride length generated by the open-loop controller is essentially influenced not only by the frequency parameter f but also by the amplitude parameter A. In particular, around the parameter space $f \simeq 0.7$ (Hz) and $0.0 < A < 6.0$ (Nm), large variations of stride length can be achieved with respect to the amplitude parameter. With smaller values of the frequency parameter (e.g. $0.5 < f < 0.6$ (Hz)), however, we cannot expect significant variations of stride length even by large changes of the amplitude parameter. In contrast, regardless of the amplitude value, it is possible to control stride length approximately between 0.15 and 0.25 (m) when the frequency parameter is varied.

It is also shown that, from the figure of phase delay (upper right plot in Fig. 4), the phase delays between mechanical dynamics and the oscillator is more significant with respect to the frequency parameter if compared with the amplitude parameter (especially at a smaller amplitude parameter, i.e. $A \simeq 2.5$ (Nm)). This essentially means that, when the robot varies the frequency parameter at a smaller amplitude parameter for a switch of stride length, it requires many leg steps for the transition between one stride length to the other.

The fix points can be also found in locomotion on inclined slopes, and Fig. 5 shows stride length $Stride^*$ with respect to the frequency parameter in various slopes (the amplitude parameter is fixed at $A = 7.0$ (Nm)). In general, it is possible to control stride length also in inclined slopes through the frequency parameter by considering the fact that stride length becomes smaller as the frequency parameter increases. However, it is generally the case that control of shorter stride is more difficult in downhill slopes ($\gamma < 0$), and longer one in uphill ($\gamma > 0$). Moreover, variations of stride lengths tend to be richer in uphill locomotion since $Stride^*$ exists between 0.10 and 0.25 (m) in the slope angle $\gamma = 0.005$ (rad), whereas it is much narrower in downhill slopes (e.g. $0.30 < Stride^* < 0.34$(m) in the slope $\gamma = -0.015$).

3 Dynamics of a Compass Gait Robot

For a real-world evaluation of the proposed control framework, we developed a robot platform based on the compass gait model with a few practical modifications. In this section, we first describe the design and control of the platform, then behavioral characteristics are analyzed through locomotion experiments.

3.1 Design and Control of Robot

The robot platform shown in Fig. 6. consists of two leg segments connected through a hip joint, where a direct-drive motor (Maxon Motor RE40 with no gear reduction) exerts torque between two legs. The hip joint is then connected to a boom that allows pitch rotation while restricting yaw and roll. At the other end of the boom, we installed a counter weight to avoid a large ground impact of every step, and of harmful crashes of the entire robot (see Table 2 for more specifications of the robot platform).

In contrast to the simulation model, foot retraction is necessary to avoid the swing leg colliding with the ground, and for this reason, each leg segment has a servomotor (Hitech HSR-5980SG) that extends and retracts a foot segment for ground clearance during swing phase. To reduce the difference in dynamics between the simulation and the real-world experiments, we minimize the mass of the foot segments such that they are negligible. Because of the foot actuation, the state variables of this platform are $q = [\theta_1, \theta_2, l_1, l_2]^T$ and their velocity

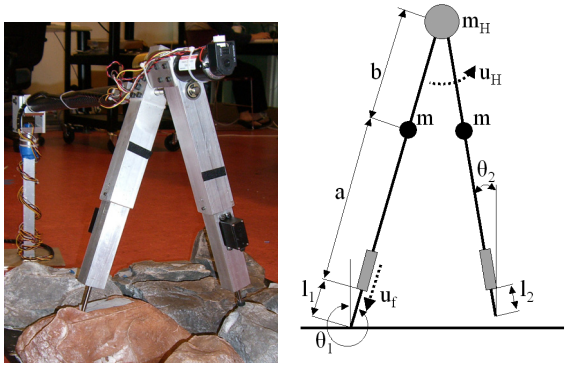

(a) (b)

Fig. 6 (a) Photograph of Compass Gait Robot, and (b) Compass Gait Model with hip and foot actuators (gray circle and rectangles).

Table 2 Specification of Robot

Symbol	Description	Value
a	Lower Leg Segments	0.260 m
b	Upper Leg Segments	0.055 m
l_1, l_2	Foot Segments	0.000-0.040 m
m	Mass of Leg	1.3 kg
m_H	Mass of Body	0.2 kg
CW	Counter Weight	$4.1kg$
$BL1$	Boom Length to Robot	$1.210m$
$BL2$	Boom Length to Counter Weight	$0.560m$
A	Amplitude of Oscillation	$1.0Nm$
$P_{i,12}$	Amplitude of Foot Extension	$0.000 - 0.015m$
ψ	Phase Delay of Foot Oscillation	$2.2rad$

components $\dot{q}$. In addition to the sinusoidal oscillation of hip motor torque described by Eq. (3), the robot receives an additional control input for control of foot actuators. The motor torque u_{fi} of the foot motor i can be described as follows:

$$u_{fi}(t) = K_p(l_i - P_{ri}(t)) + K_d(\dot{l}_i - 0.0), \quad (9)$$

$$P_i(t) = \begin{cases} P_{i1} : \sin(2\pi ft + \psi) > 0 \\ P_{i2} : otherwise \end{cases} \quad (10)$$
$$(i = 1, 2)$$

where K_p and K_d are the proportional and differential gains of PD controller, and $P_{i\{1,2\}}$ represents the given setpoints of the foot segment i.

For sensory feedback and measurement of locomotion dynamics, we implemented an encoder at the hip motor (Maxon Motor HEDS5540), force sensitive resistors in both foot segments, and a potentiometer that measures horizontal position around the boom. These motors and sensors are connected to a PC104 computer (Digital-Logic MSM-P5SEN) with a sensor board (Sensoray Model-526), which enables the control bandwidth

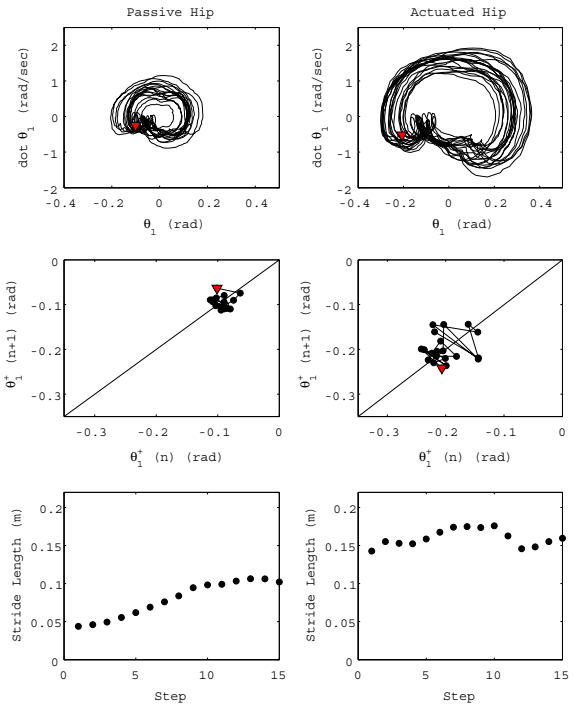

Fig. 7 Basin of attraction with and without hip actuation. Phase plots (top), return maps of the robot's outer leg (middle), and corresponding stride length (bottom). Red triangles denotes the beginning of data recording.

of approximately 100 Hz. In addition, in order to measure the overall dynamics of the robot during locomotion, we conducted the experiments under the motion capture systems (Vicon MX consisting of 16 cameras, which use infrared light to track reflective markers on the robot at approximately 120Hz sampling rate).

3.2 Steady State Dynamics

When we properly set the control parameters described in the previous section, the compass gait robot exhibits stable periodic walking gait on a flat terrain. In order to characterize basic behaviors of the robotic platform, the first set of experiments were conducted on a flat terrain with a few different configurations of control parameters.

Fig. 7 shows a phase plot and return map of one of the legs, and stride length of every step with and without the hip motor control. As shown in the left plots of Fig. 7, the basic locomotion dynamics of the compass gait robot can be generated simply by using the foot segment control without hip actuation (i.e. $u_H = 0.0$). Specifically, even with an initial condition

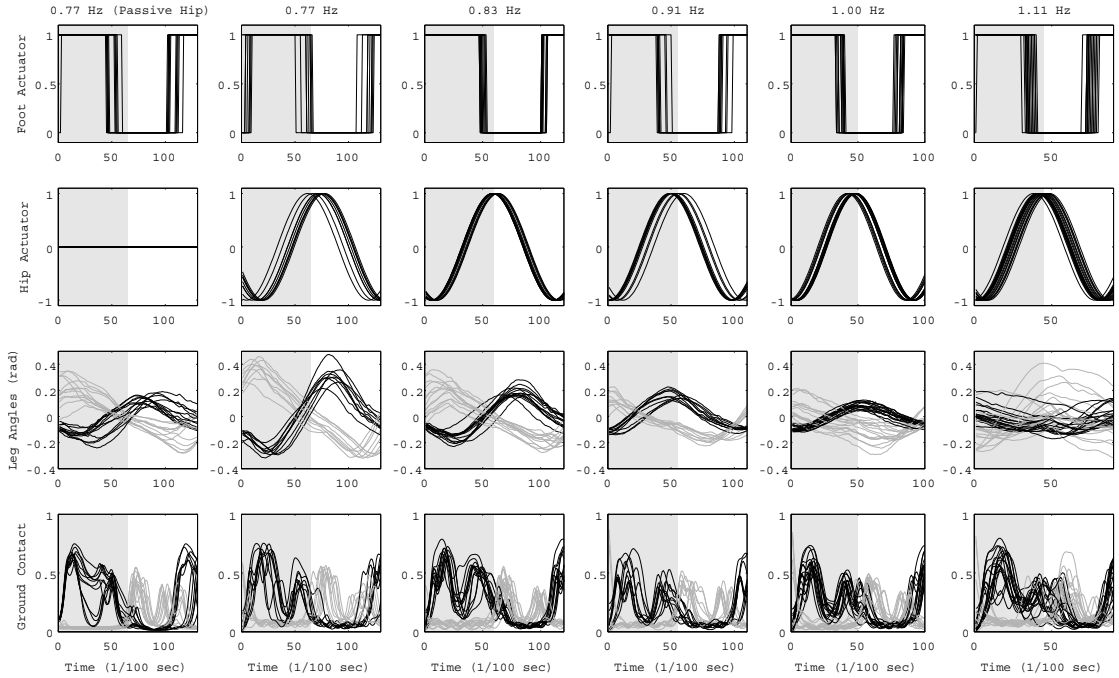

Fig. 8 Time series trajectories of walking dynamics with different frequency parameters. Experimental data of 10 steps are aligned with respect to the ground reaction force of a leg. The gray rectangles in each plot represents the stance period of a leg based on the ground reaction force. The trajectories of foot and hip actuators, and the ground reaction force are normalized.

of $[\theta_1, \theta_2, \dot{\theta_1}, \dot{\theta_1}]^T = [0, 0, 0, 0]^T$, walking dynamics of the robot reaches a limit cycle of dynamics resulting in steady stride length after several steps. While this walking dynamics is relatively stable on a flat terrain, the walking direction is not controllable (the limit cycle of forward or backward walking is largely dependent on the initial conditions and environment), and the robot is not able to walk uphill. In contrast, with the hip actuation (Fig. 7 right plots), we can observe a similar limit cycle of locomotion, but the amplitude and the perturbation of leg swing are much larger resulting in the longer stride.

Fig. 8 shows trajectories of the motor command $[u_H, u_{f1}]^T$ and the state variables $q = [\theta_1, \theta_2]^T$ of successive ten steps, which are aligned with respect to the ground contact detected by the foot pressure sensor. Despite some differences between dynamics of the simulation model and the robotic platform, we can clearly observe some of the salient characteristics that we found in the simulation analyses. First, in the plots of foot and hip actuators of Fig. 8, phase locking can be found by comparing the oscillation cycle and the periods of stance phase: on the one hand, the oscillation cycles are synchronized with the stance phases (gray regions in the plots), and on the other, the peaks of oscillation tend to be advanced as the frequency parameter increases. And second, amplitude of swing legs is much larger at smaller frequency parameters, which was also the case in Fig. 3 (lower figures).

3.3 Gait Variability

As in the simulation analysis, we also conducted a set of experiments to examine stride length with respect to the frequency parameter of the oscillator and the slope angles. Fig. 9 (the filled circle plots) shows the mean stride length and standard deviation of ten steps of walking with respect to the set of frequency parameter. From this figure, it is possible to increase stride length of the steady state locomotion approximately 50% by changing the frequency from 1.11 to 0.77 Hz.

The same set of frequency parameters was also tested in different inclinations of slopes in order to analyze controllability of foot placement in rough terrains. Fig. 8 shows that the robot is able to walk with different stride length in large variety of slopes (between +5 and -7 degrees). On the level ground, the variability of stride length is between approximately 0.09 and 0.15 m. With the same range of the frequency parameter, the stride length becomes larger in downhill, and smaller in uphill

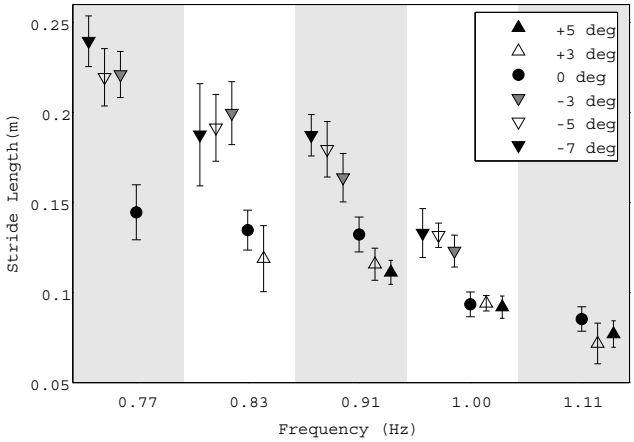

Fig. 9 Variability of stride with respect to five frequency parameters in the different inclinations of slope (downhill -3, -5, -7 degrees, level ground, and uphill: +3 and +5 degrees). Every plot represents a mean stride length of 10 steps and their standard deviation in each environment.

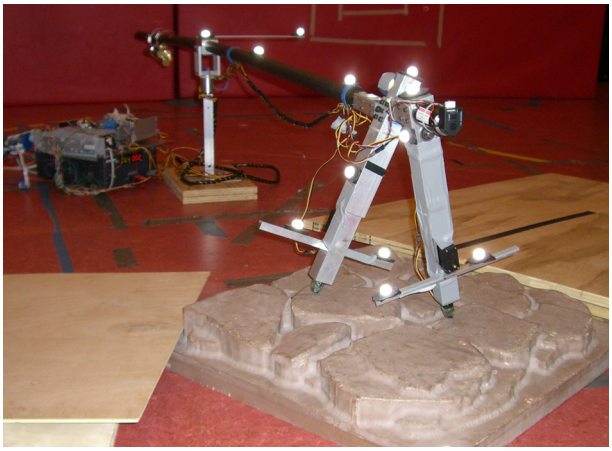

Fig. 10 Rough terrain experiment with the motion capture system. 12 markers are attached in the boom and legs.

environments. An important characteristic of the proposed control architecture is the fact that the robot is not able to walk uphill with the lower frequency of oscillator, and downhill with the higher frequency. More specifically, the +5 degree uphill can be dealt with by the frequency of 0.83Hz and larger, and the robot can walk down -7 degree slope with the frequency of 1.0Hz or lower. In other words, the limit of the proposed controller is the control of small stride in downhill, and large stride in uphill.

4 Locomotion Control in Rough Terrain

One of the most significant advantages of the proposed control architecture lies in the fact that, by exploiting the self-stability, one control parameter is sufficient to vary the basic walking dynamics, and as a result, optimization of the feedback control to deal with rough terrains can be significantly simpler. This section explains how the aforementioned open-loop controller can be extended with a sensory feedback about the environment, and analyzes the performance of locomotion in a rough terrain.

4.1 Feedback Controller

For the sake of simplicity, we assume that the feedback controller receives only the location of horizontal axis every control step, and determines the frequency value of the oscillator. The feedback controller, therefore, can be described as

$$f = freq(x, t) \tag{11}$$

where x represents the current horizontal position of the hip joint with respect to an absolute coordinate system. The function $freq(x, t)$ also depends on the time variable of oscillator, because the controller is allowed to change the frequency only at the end of every oscillation period for smooth transitions of motor command.

In the following case study, we heuristically determined the function $freq(x, t)$ for a given rough terrain. Owing to the minimalistic control architecture, it requires only several trials and errors until we found a set of thresholds for the parameter x for multiple successful travels over the rough terrain.

4.2 Experiments

The rough terrain that we tested in this case study consists of a flat terrain, an uphill slope, molded "flat rocks", and a downhill as shown in Fig. 10 and 11. The important features of this terrain are a +3.75 degree uphill, -2.60 degree downhill, 0.60m of rough terrain with the largest gap length of 0.03m and the largest step hight of +0.02m and -0.03m.

After several trials and errors, we set the control parameters as follows:

$$freq(x,t) = \begin{cases} 0.77 \text{ Hz} : x < 3.4m \\ 1.11 \text{ Hz} : x \geq 3.4 \text{ and } x < 4.5m \\ 1.00 \text{ Hz} : x \geq 4.5 \text{ and } x < 5.1m \\ 0.77 \text{ Hz} : x \geq 5.1m \end{cases} \tag{12}$$

More specifically, based on the basic knowledge about the gait variability (shown in Fig. 9), we set the frequency parameter to a larger value for the uphill slope,

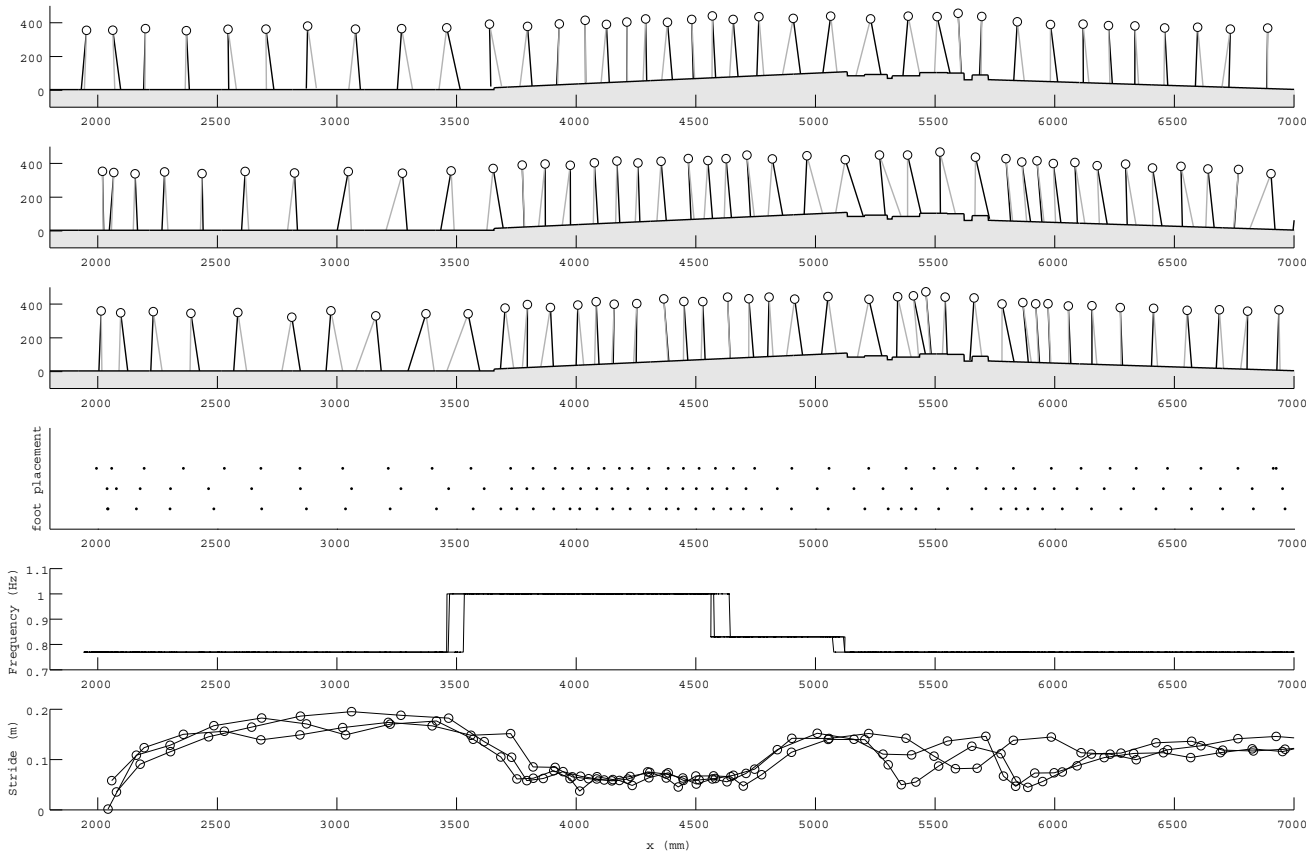

Fig. 11 Walking experiments in rough terrain. Top figures show the trajectories of the three successful travels of the rough terrain. The location and pose of the robot are depicted every 0.8 second. The dots in the middle plot represent foot placement over three successful trials. The lower plots show the frequency parameter of oscillator, and the stride length of every step during the three successful trials.

and set to a smaller frequency for larger strides in the downhill slope and flat surfaces.

This controller was tested under the motion capture system to record the kinematics of the robot, and three successful travels over the rough terrain are reproduced in Fig. 11. In general, the controller is able to maintain the locomotion mostly on the flat surfaces including the uphill, the downhill, and the small step around $x = 3.6m$. It is important to note that, even though there are some variance in the foot placement, the controller is able to cope with locomotion over sparse gaps and steps on the ground by appropriately setting the function $freq(x, t)$. Note also that the stride length with respect to the frequency parameter is mostly comparable to the steady state locomotion experiments in Fig. 9 (i.e. 0.19m stride length at the frequency of 0.77Hz, and 0.05m at 1.11Hz, for example).

The limitation of the controller, however, is that it occasionally failed on the rocks ($x = 4.9 - 5.5m$). Considering the large variance of stride length in this area of the terrain shown in Fig. 11, the main reason of failures seems to be originated in the irregular ground interactions.

5 Conclusion

This paper presented a minimalistic control architecture for dynamic walking of the compass gait model. The controller makes use of an open-loop sinusoidal oscillation at the hip joint, and we identified the phase locking mechanism that self-calibrates phase delays between walking dynamics and oscillation of the hip motor. This mechanism can be nicely explained by a fix point analysis, by which we could also systematically investigate the relation between walking dynamics and the motor control parameters. The main contribution of this paper lies in the fact that, owing to the phase locking mechanism, a simple open-loop based controller can deal with various uneven terrains such as steady walking in uphill and downhill slopes as well as controlling foot placement to deal with gaps and steps. This minimalistic controller is particularly important

for planning and optimization of locomotion control in moderately complex environment. In the case study we showed in Section 4, for example, it required only several trials and errors until we found the set of parameters. It should, therefore, be straight forward to automate the search process of control parameters by using a depth-first algorithm, for example.

For dynamic locomotion in more complex environment, however, we also identified a few potential limitations of the proposed control framework. First, as shown in the simulation of Section 2.3 and the real-world experiment of Section 3.2, controllability of stride length is degraded as the angle of slope increases for both uphill and downhill. And second, in the proposed control approach, it requires several steps until a stride length converges to another when switching the control parameter of the oscillator. For example, in the upper plots of Fig. 3, it took approximately three to ten steps until it converges to a steady stride length when the simulated compass gait model started with various initial conditions. And in Fig. 11, we also observed three to five steps of transition steps when the controller switched the parameter in the real-world platform.

To cope with these open problems, we expect two future research directions based on our achievement presented in this paper. One of the potential extensions of the proposed controller is to examine the effects of different oscillator trajectories. For example, although we tested only control of frequency parameter in this paper, the amplitude parameter of the oscillator could potentially provide an additional increase of controllability as our simulation analysis suggested in Section 2.3. Second, it is also important to pursue the use of sensory feedback in the low-level controller. In particular, it is interesting to investigate further how the phase locking mechanism identified in this paper is related to phase resetting triggered by a feedback controller, which is often used in the central pattern generator models [33, 36, 37], for example. In addition, it is also interesting to consider how the phase locking mechanism can be integrated into a more comprehensive optimization process of state-feedback controllers as demonstrated in [34, 35], for example.

Acknowledgements This work is supported by the National Science Foundation (Grant No. 0746194).

References

1. McGeer, T. (1990). Passive dynamic walking. International Journal of Robotics Research, 9(2):62.82, April 1990.
2. Collins, S. H., Wisse, M., and Ruina, A. (2001). A three-dimentional passive-dynamic walking robot with two legs and knees. *International Journal of Robotics Research* 20, 607-615.
3. Collins, S. H., Ruina, A., Tedrake, R., and Wisse, M. (2005). Efficient bipedal robots based on passive-dynamic walkers. Science, Vol. 307, 1082-1085.
4. Wisse, M. and van Frankenhuyzen, J. (2003). Design and construction of MIKE: A 2D autonomous biped based on passive dynamic walking. *Proceedings of International Symposium of Adaptive Motion and Animals and Machines (AMAM03).*
5. Tedrake, R., Zhang, T.W. and Seung, H.S. (2004). Stochastic policy gradient reinforcement learning on a simple 3D biped. Proceedings of the IEEE International Conference on Intelligent Robots and Systems (IROS), volume 3, pages 2849-2854
6. Tedrake, R. (2004). Applied optimal control for dynamically stable legged locomotion. PhD thesis, Massachusetts Institute of Technology, 2004.
7. Iida, F., Rummel, J., and Seyfarth, A. (2008). Bipedal walking and running with spring-like biarticular muscles, Journal of Biomechanics, Vol. 41, 656-667.
8. Hobbelen, D.G.E, and Wisse, M. (2008). Swing-leg retraction for limit cycle walkers improves disturbance rejection, IEEE Transactions on Robotics, Vol. 24, No. 2, 377-389.
9. Kajita, S., Espiau, B. (2008). Legged robots, In: Springer Handbook of Robotics, Siciliano, B. and Khatib, O. (Eds.), 361-389.
10. Garcia, M., Chatterjee, A., Ruina, A., and Coleman, M. (1998). The simplest walking model: Stability, complexity, and scaling. Journal of Biomechanical Engineering . Transactions of the ASME, 120(2), 281-288.
11. Goswami, A., Thuilot, B., and Espiau, B. (1998). A study of the passive gait of a compass-like biped robot: Symmetry and chaos, International Journal of Robotics Research, Vol. 17(12), 1282-1301.
12. van der Linde, R.Q. (1999). Passive bipedal walking with phasic muscle contraction, Biological Cybernetics, 81: 227-237.
13. Miyakoshi, S., Cheng, G. (2004). Examining human walking characteristics with a telescopic compass-like biped walker model, Proceedings of the IEEE International Conference on Systems, Man and Cybernetics (SMC2004), 1538-1543.
14. Asano, F., Hayashi, T., Luo, Z.W., Hirano, S., Kato, A. (2007). Parametric excitation approaches to efficient dynamic bipedal walking, Proc. of the IEEE/RSJ Int. Conf. on Intelligent Robots and Systems, 2210-2216.
15. Harata, Y., Asano, F., Luo, Z.W., Taji, K., Uno, Y. (2007). Biped gait generation based on parametric excitation by knee-joint actuation, Proc. of the IEEE/RSJ Int. Conf. on Intelligent Robots and Systems, 2198-2203.
16. Kinugasa, T., Miwa, S., Yoshida, K. (2008). Frequency analysis for biped walking via leg length variation, Robotics and Mechatronics, 20(1): 98-104.
17. Kuo, A.D. (2002). Energetics of actively powered locomotion using the simplest walking model, Journal of Biomechanical Engineering, Vol.124, 113-120.
18. Ono, K., Furuichi, T., Takahashi, R. (2004). Self-excited walking of a biped mechanism with feet, International Journal of Robotics Research, 23(1): 55-68.
19. Adamczyk, P.G., Collins, S.H., Kuo, A.D. (2006). The advantages of a rolling foot in human walking, Journal of Experimental Biology, 209: 3953-3963.
20. Kim, J. Choi, C., Spong, M. (2007). Passive dynamic walking with symmetric fixed flat feet, International Conference on Control and Automation, 24-30.
21. Kwan, M., Hubbard, M. (2007). Optimal foot shape for a passive dynamic biped, Journal of Theoretical Biology, 248: 331-339.
22. Hass, J., Herrmann, J.M., Geisel, T. (2006). Optimal mass distribution for passivity-based bipedal robots, International Journal of Robotics Research, 25(11): 1087-1098.

23. Kuo, A.D. (1999). Stabilization of lateral motion in passive dynamic walking, International Journal of Robotics Research, 18(9): 917-930.
24. McGeer, T. (1988). Stability and control of two-dimensional bipedal walking. Simon Fraser University CSS-ISS TR 88-01.
25. Goswami, A., Espiau, B., Keramane, A. (1997). Limit cycles in a passive compass gait biped and passivity-mimicking control laws, Autonomous Robots, 4:273-286.
26. Asano, F., Yamakita, M., Furuta, K. (2000). Virtual passive dynamic walking and energy-based control laws, IEEE/RSJ International Conference on Intelligent Robots and Systems (IROS 2000), 1149-1154.
27. Spong, M.W. (2003). Passivity based control of the compass gait biped, In: IFAC World Congress, 19-24.
28. Spong, M.W. and Bhatia, G. (2003). Further results on control of the compass gait biped. In Proceedings of the IEEE International Conference on Intelligent Robots and Systems (IROS), 1933-1938.
29. Asano, F., Yamakita, M., Kamamichi, N., and Luo, Z-W, (2004). A novel gait generation for biped walking robots based on mechanical energy constraint, IEEE Transactions on Robotics and Automation, Vol. 20(3), 565-573.
30. Pekarek, D., Ames, A.D., Marsden, J.E. (2007). Discrete mechanics and optimal control applied to the compass gait biped, Proceedings of IEEE Conference on Decision and Control, 5376-5382.
31. Kurz, M.J., Stergiou, N. (2005). An artificial neural network that utilizes hip joint actuations to control bifurcations and chaos in a passive dynamic bipedal walking model, Biological Cybernetics, 93: 213-221.
32. Aoi, S. and Tsuchiya, K. (2006). Stability analysis of a simple walking model driven by an oscillator with a phase reset using sensory feedback, IEEE Transactions on Robotics, 22(2): 391-397.
33. Aoi, S. and Tsuchiya, K. (2007). Self-stability of a simple walking model driven by a rhythmic signal, Nonlinear Dynamics, 48(1), 1-16.
34. Byl, K., and Tedrake, R. (2008). Metastable walking on stochastically rough terrain. In Proceedings of Robotics: Science and Systems IV, 2008.
35. Byl, K. and Tedrake, R. (2008). Approximate optimal control of the compass gait on rough terrain. In Proceedings IEEE International Conference on Robotics and Automation (ICRA), 1258-1263.
36. Taga, G., Yamaguchi, Y., and Shimizu, H. (1991). Self-organized control of bipedal locomotion by neural oscillators in unpredictable environment. Biological Cybernetics 65, 147-159.
37. Manoonpong, P., Geng, T., Kulvicius, T., Porr, B., Wörgötter, F. (2007). Adaptive, fast walking in a biped robot under neuronal control and learning, PLoS Computational Biology, 3(7): 1305-1320.